Desalination and Water Treatment
www.deswater.com
doi: 10.1080/19443994.2013.870748

53 (2015) 2464–2480
March

Taylor & Francis
Taylor & Francis Group

Ion-exchange properties of ternary CaO–MgO–Al_2O_3 spinels in pH-controlled aqueous radioactive waste solutions

B. El-Gammal[a,*], M. Abdel Hamid[a], G.M. Ibrahim[a,b,1]

[a]*Hot Laboratories Center, Atomic Energy Authority, P. No. 13759, Cairo, Egypt*
Email: belalelgammal@hotmail.com
[b]*King Khalid University, Bisha Branch, Bisha, Kingdom of Saudi Arabia*

Received 3 January 2013; Accepted 30 October 2013

ABSTRACT

Spinel ion-exchange materials, composed of CaO–MgO–Al_2O_3 ternary systems were prepared via sol–gel reactions followed by sintering at different temperatures. $Ca_3MgAl_4O_{10}$, $Ca_3Al_2O_6$, $CaMg_2Al_{16}O_{27}$, $Ca_2Mg_2Al_{26}O_{45}$, corundum, periclase, and monoxide lime were detected at room temperature, while $CaAl_2O_4$ and $MgAl_2O_4$ spinels were ascertained at 1,200–1,400 and 1,725–1,900°C, respectively. They were characterized using scanning electron microscopy, X-ray diffraction, X-ray fluorescence, FTIR, DTA–TGA, N_2-gas adsorption, and laser diffraction particle size analyzer. We proved that they are chemically and thermally stable in their face-centered array spinel configurations with different surface, morphological, and topographical structures. They were used for removal of $^{134}Cs^{+}$, $^{60}Co^{2+}$, and $^{152-154}Eu^{3+}$ from waste solutions; preliminary kinetic and pH were investigated. Langmuir, Freundlich, Dubinin–Radushkevich, Temkin, Harkins–Jura, and Halsey isothermal prototypes were applied to describe the equilibria between adsorbed phase metal ions and those in solution at different concentrations. The adsorption of $^{134}Cs^{+}$, $^{60}Co^{2+}$, and $^{152-154}Eu^{3+}$ was critically affected by temperatures and ambient pH; spontaneous and exothermic nature of adsorption was found at specific pH values, beyond which the adsorption is restricted. The mechanism of adsorption was found to be chemical reaction combined with ion exchange rather than pure ion exchange.

Keywords: Ion exchange; CaO–MgO–Al_2O_3 spinels; Cesium; Cobalt and europium

1. Introduction

The necessity for dealing with radioactive $^{134}Cs^{+}$, $^{60}Co^{2+}$, and $^{152-154}Eu^{3+}$ has consistently been exigent since the diffusive radionuclides of high activity put forward a threat toward the biosphere. Competent and selective separation or removal of the key radionuclides $^{134}Cs^{+}$, $^{60}Co^{2+}$, and $^{152-154}Eu^{3+}$ from the fission product soup prior to dealing with long-lived radioactive aqueous effluents arising from weapon production, nuclear power and reprocessing plants, and medical isotope production has unfailingly been a significant confrontation around the world. Although

*Corresponding author.

[1]Current address: King Khaled University, Bisha Branch, Bisha, Kingdom of Saudi Arabia.

the traditional solvent extraction has been widely used in spent nuclear fuel processing [1,2], inorganic materials are preferred over the organic systems because the environmentally sound approach acquires the simplicity in disposing the material, the reliability of resisting to radiation, and the capability of achieving a superior selectivity. Both natural and synthetic ion exchangers have been studied for the retention of $^{134}Cs^{+}$, $^{60}Co^{2+}$, and $^{152-154}Eu^{3+}$ in past decades. However, their efficient application has been confined to the decontamination of cesium from the neutral, low-salt solution [3,4]. Subsequently, microporous silicotitanates (IONSIV IE-911, ETS-4/10) have been synthesized and evaluated as selective ion exchangers for Cs^{+} and Sr^{2+} in simple non-basic simulants [5–7].

Meanwhile, antimony-based pyrochlores (antimony silicate) [8] and tungsten oxides (hexagonal tungsten bronze structures) [9], typical of hydrous metal oxides, are reported to show a considerable affinity toward cesium or strontium in the acidic media. However, the Cs^{+} and Sr^{2+} in those low-acidic solutions were presented at only trace level. Others, encouraging results with ammonium molybdophosphate/transition metal hexacyanoferrate immobilized on diverse supports (mesoporous silica and polymer resins), presented as bulk materials or nanocomposites were reported for the decontamination of cesium ions recently [10–15]; however, they have questionable thermal stability at the elevated temperatures generated by decay energy. Ternary acidic salts of multivalent metal were used to achieve the analytical separations of heavy-metal ions [16–18], few of which were focused on the removal of Cs^{+} and Sr^{2+}. Generally, the extreme conditions of the high-level liquid waste have been disabling any material to separating both cations from other radionuclides commendably. In a recent development, spinel structures were used to remove some monovalent ions from waste streams; correlation between Li^{+} adsorption capacity and the preparation conditions of spinel lithium manganese precursor was conducted [19]. On the other hand, *in situ* monitoring of the adsorption of Co^{2+} on the surface of Fe_3O_4 was recently discovered [20]. Structural analyses using extended X-ray absorption fine structure and high-resolution transmission electron microscope show that the inverse spinel structure is preserved in the Co-incorporated surface atomic layers of the Fe_3O_4 nanoparticles. These results suggest that the dissolved radioactive isotope ^{60}Co in the primary cooling loop of supercritical water-cooled nuclear reactors has a high likelihood of precipitating on the surfaces of ferrite nanomaterial nanoparticles in high-temperature aqueous fluids [20].

In the current study, different spinels' structures based on the CaO–MgO–Al_2O_3 ternary systems were prepared and checked as chemically and thermally stable spinels, in order to remove $^{134}Cs^{+}$, $^{60}Co^{2+}$, and $^{152-154}Eu^{3+}$ from waste streams.

2. Experimental

2.1. Chemicals and instrumentations

All chemicals and reagents were of analytical grade. Calcium chloridedihydrate, $CaCl_2H_4O_2$ has 147.014 g mol^{-1} as molecular weight; magnesium chloride hexahydrate, $Cl_2H_{12}MgO_6$ with 203.302 g mol^{-1}; and aluminum secondary butylate, $C_{12}H_{27}AlO_3$, having 246.322 g mol^{-1}; were obtained from Loba Chemie, Germany. Europium nitrate [$Eu(NO_3)_3$] was purchased from Aldrich Chem. Cobalt chloride, as $CoCl_2$ and cesium chloride as CsCl were obtained from Fisher Scientific Co., USA. $^{134}Cs^{+}$, $^{60}Co^{2+}$, and $^{152-154}Eu^{3+}$ were available by irradiating the suitable corresponding salts in the Egyptian research reactor at Inshas site.

2.2. Preparation of CaO–MgO–Al_2O_3 spinels

The CaO–MgO–Al_2O_3-based spinels were prepared by mixing $CaCl_2H_4O_2$, $Cl_2H_{12}MgO_6$, and $C_{12}H_{27}AlO_3$ in 1:1:1 M ratio after suitable dilution using isoprpopyl alcohol as a common polar solvent. The mixture was stabilized using HCl and later stirred at 70°C for 120 min. The obtained sols were gelated using liquid ammonia for 4 h, afterwards filtered, and washed to get rid of free nitrate ions with demineralized water (pH ~4). The product was dried at room temperature and treated with 1 M HNO_3 for 24 h to convert it into the H-form with occasional shaking and intermittently replacing the supernatant liquid with fresh acid. The material obtained was washed with demineralized water to remove the excess acid and dried at 45°C. Later on, the produced formulations must be subjected to the suitable heat treatments in order to get the final spinels.

Figs. 1–4 show the effect of temperature on the spinel formation. As it could be seen in Fig. 1, no spinel structures could be observed via the normal sol–gel route from 25 to 1,200°C. Some chemical formulations, namely, $Ca_3MgAl_4O_{10}$, $Ca_3Al_2O_6$, $CaMg_2Al_{16}O_{27}$, $Ca_2Mg_2Al_{26}O_{45}$, corundum, periclase, and monoxide lime were observed and elucidated using energy dispersive X-ray fluorescence (ED-XRF). On raising the sintering temperature in the range 1,200–1,900°C, Figs. 2–4, the quantity of produced spinel was proportional to spinel area in the figures, which is consequently proportional to the temperature rising. The $CaAl_2O_4$ spinel was firstly detected at

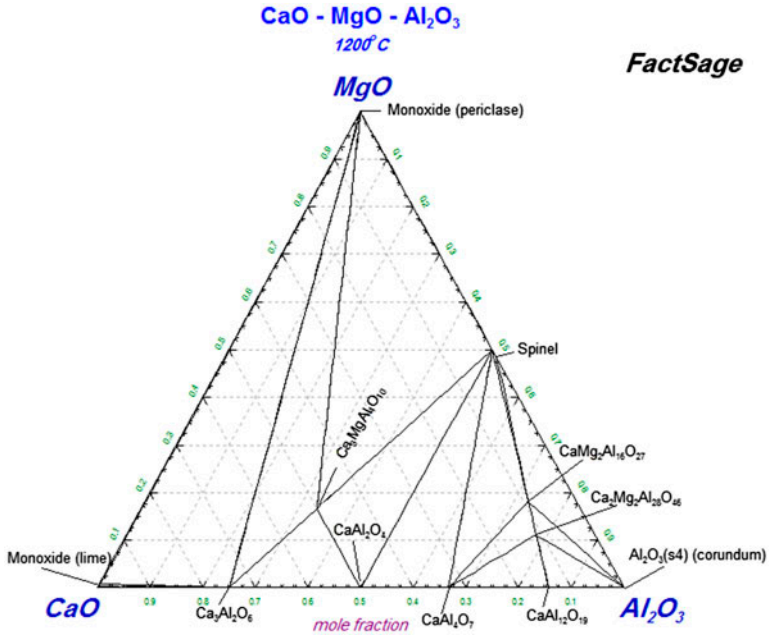

Fig. 1. Phase diagram of CaO–MgO–Al_2O_3 ternary system at 1,200˚C.

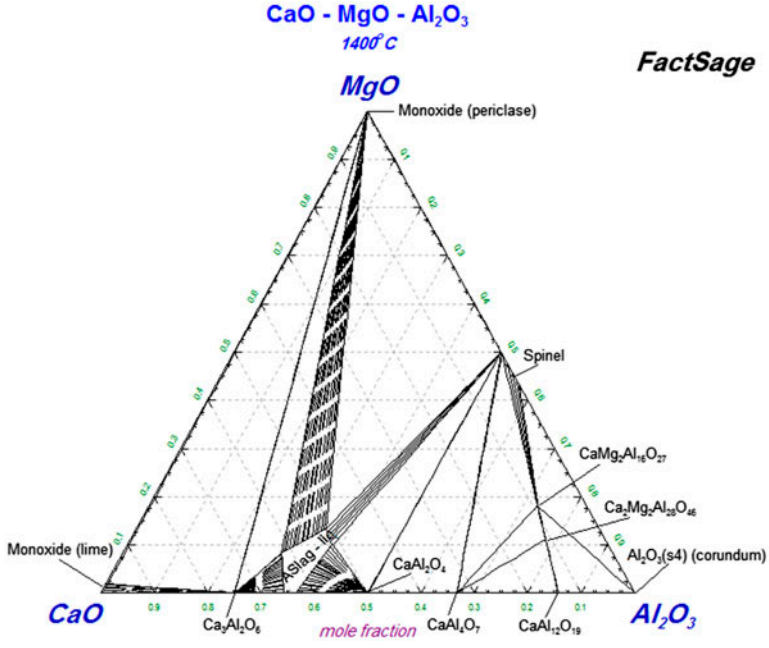

Fig. 2. Phase diagram of CaO–MgO–Al_2O_3 ternary system at 1,400˚C.

about 1,200˚C. On the other hand, $MgAl_2O_4$ spinel appeared from 1,725 to 1,900˚C. The obtained spinels were later ground and sieved to different mesh sizes; 60–80 mesh sizes were used during batch experiments.

2.3. Characterization

The prepared spinels were characterized by advanced analytical techniques. Simultaneous DTA–TGA system, type DTA–TGA-50, Shimadzu, Japan, was used to

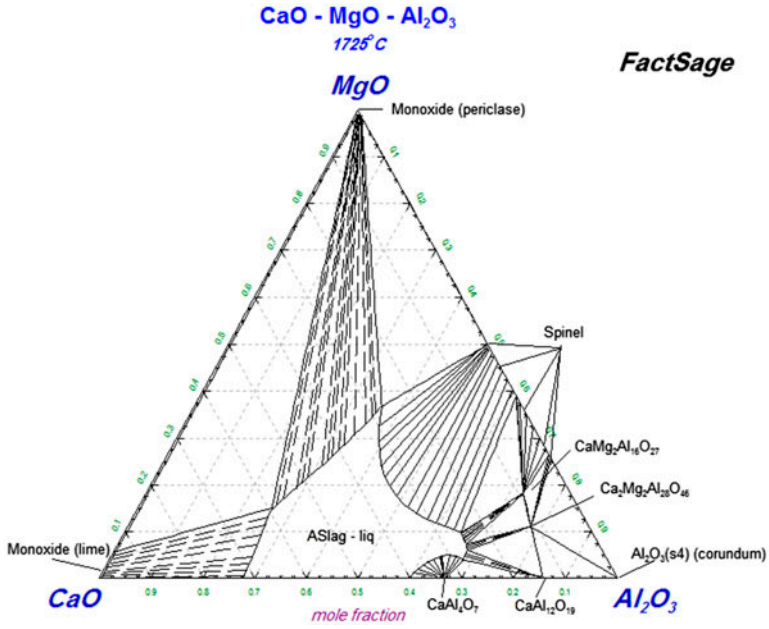

Fig. 3. Phase diagram of CaO–MgO–Al_2O_3 ternary system at 1,725˚C.

measure phase changes and weight losses from the sample, respectively, at heating rate of 10˚C min^{-1} under nitrogen gas to avoid thermal oxidation of the spinel powders.

The morphology of the prepared spinels was studied using scanning electron microscopy (SEM, model JSM 5400, JEOL, USA). Samples were washed, dried and mounted on the support and then made conductive with sputtered gold.

Powder X-ray diffraction (XRD, model XD610, Shimadzu, Japan) data used for least-squares refinements of lattice parameters were recorded on an X-ray diffractometer, at room temperature, using Bragg–Brentano geometry, with a back-monochromatized Cu Kα radiation. Samples were ground and mounted on a flat sample plate. The diffraction pattern was scanned over the angle range 4–90 (2θ) in step of 0.031 (2θ) and a counting time of 10 s per step. The unit-cell parameters were refined by a least-squares procedure.

ED-XRF (ZT2830 XRF, PANalytical, USA) was used as the simplest, most accurate, and most economic analytical method for determination of the chemical composition of the prepared spinels. It is non-destructive and reliable, requires no, or very little, sample preparation and is suitable for solid, liquid, and powdered samples with detection limits up to 100%.

Perkin–Elmer FTIR, model BXII, USA, in the range 500–4,000 cm^{-1} was cast off to identify the IR spectrum of the different spinels activating the disc technique. In this concern, every sample was thoroughly mixed with KBr as a matrix, and the mixture was ground and then pressed with a special press to give a disc of standard diameter.

Laser diffraction particle size analyzer (SALD 2001, Shimadzu, Japan) was used to distinguish between the different mesh sizes obtained as well as their distributions.

Textural characterizations of the different spinels were carried out by N_2 adsorption at 77 K using Autosorb I, supplied by Quantachrome Corporation, USA. The BET (N_2, 77 K) is the most usual standard procedure used when characterizing these spinels. From the BET plots the surface area, S_{BET}, the total pore volumes estimated from the volume of N_2 adsorbed at $p/p° = 0.95$, V_t, and an average pore radius from $r_a = 2V_p/S_{BET}$ were found to be (234.76 m^2 g^{-1}, 0.1765 mL g^{-1}, and 15.08 Å) and (387.56 m^2 g^{-1}, 0.1942 mL g^{-1}, and 10.08 Å) for $MgAl_2O_4$ and $CaAl_2O_4$, respectively.

2.4. Ion-exchange studies

Batch ventures were carried out in 250 mL Erlenmeyer flasks containing 50 mL of known concentrations of $^{134}Cs^+$, $^{60}Co^{2+}$, and $^{152-154}Eu^{3+}$ solutions and amount of spinel with a constant shaking speed of 125 rpm for a defined time period. To optimize the conditions for maximum $^{134}Cs^+$, $^{60}Co^{2+}$, and $^{152-154}Eu^{3+}$ removal, different sorption affecting parameters were investigated including pH (the pH of each solution was adjusted with 1 M HCl or 1 M NaOH providing a range from 2 to 9), spinel amount (0.05–0.3 g), initial

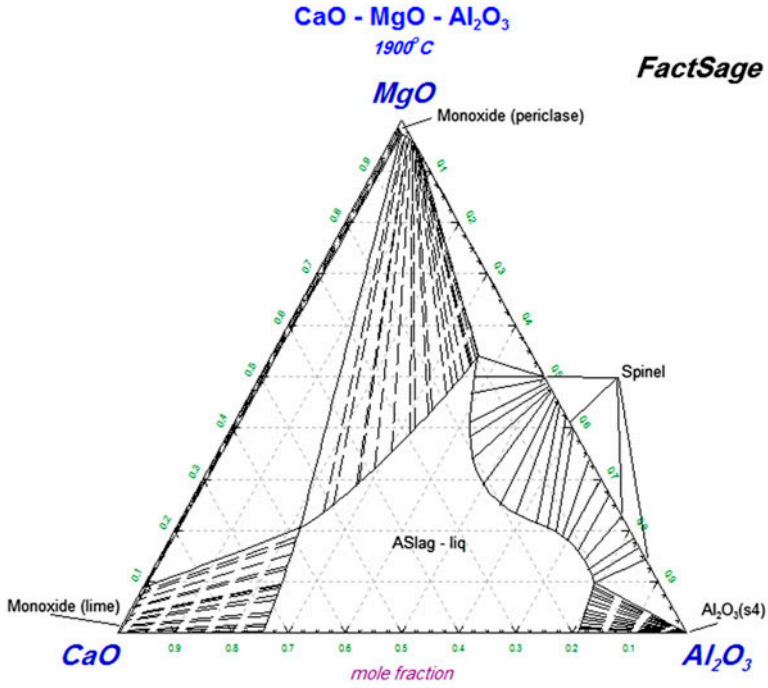

Fig. 4. Phase diagram of CaO–MgO–Al_2O_3 ternary system at 1,900˚C.

metal ion concentration (5–100 mg L^{-1}), contact time (2–800 min), and temperature (30–60˚C). After shaking, the solution was filtered and the $^{134}Cs^{+}$, $^{60}Co^{2+}$, and $^{152-154}Eu^{3+}$ concentrations were determined using the appropriate method.

The ion-exchange capacities of the $^{134}Cs^{+}$, $^{60}Co^{2+}$, and $^{152-154}Eu^{3+}$ ions were determined by shaking 10 mL of 10^{-4} M sample solution with 0.05 g of CaO–MgO–Al_2O_3 until it reached equilibrium, at room temperature. The liquid and the solid phases were separated, and then the metal ion concentration was measured in the liquid phase to calculate the percent uptake, Eq. (1). Another 10 mL of sample solution was added to the powder phase, and by repeating these steps several times and calculating the percent uptake in each case no uptake was obtained. The ion exchange capacity (IEC) was determined using Eqs. (2) and (3).

$$\%\,\text{Uptake} = \frac{C_0 - C_e}{C_0} \times 100 \tag{1}$$

$$\text{Capacity} = \frac{\sum \%\text{uptake}}{100} \times \frac{V}{m} \times C_0 \tag{2}$$

$$q_e = [C_0 - C_e] \times \frac{V}{m} \tag{3}$$

where C_0 and C_e are the initial and the measured concentrations (mmol L^{-1}) of the tested ion, V is the volume of solution (L), m is the weight of exchanger (g), and q_e is the quantity ion in mg adsorbed per one gram of the exchanging spinel.

The concentrations of cesium and cobalt ions were determined using atomic absorption spectrophotometer

Table 1
Chemical stability of CaO–MgO–Al_2O_3 spinels in different aqueous media

	Solubility %										
		HNO_3, M					HCl, M				
Sample	H_2O	0.1	0.5	1	2	4	0.1	0.5	1	2	4
$MgAl_2O_4$	B.D	B.D	B.D	2.23	3.57	5.78	B.D	B.D	B.D	1.94	**4.76**
$CaAl_2O_4$	B.D	B.D	B.D	1.25	2.94	4.91	B.D	B.D	2.3	3.49	**3.89**

B.D: below detection.

(AAS, model 210 VGP, Buck Scientific USA). Europium ion was measured by an UV–visible spectrophotometer (UV, model UV-160 A, Shimadzu, Japan). However, the concentration of $^{134}Cs^{+}$, $^{60}Co^{2+}$, and $^{152-154}Eu^{3+}$ radioactive cations were determined using NaI(Tl) scintillation detector connected to an ORTEC assembly (Nuclear Enterprises), USA.

3. Results and discussion

3.1. Characterization of the prepared material

3.1.1. Chemical dissociation studies

The chemical stability of the different spinels was studied in demineralized water, HNO_3 and HCl at 0.1, 0.5, 1, 2, and 4 M, by mixing 100 mg of each of the prepared spinels and 100 mL of the testing solution with intermittent shaking for about one week at 25 ± 1˚C. The filtrate was checked using ICP, while the solid content was gravimetrically investigated. The results are represented in Table 1.

The spinels are non-soluble in demineralized water; they can withstand the effect of acids to a great extent; they are resistant to 5 M HNO_3 and 5 M HCl. The resistance of the spinels to solubility in HCl was greater than in HNO_3. Furthermore, the chemical stability order was $CaAl_2O_4$/HCl > $MgAl_2O_4$/HCl > $CaAl_2O_4$/HNO_3 > $MgAl_2O_4$/HNO_3. Considering the detection limit, this order may be slightly different; generally, the prepared spinels have high chemical stabilities compared to cerium titanate, which has solubility percentage at 3 M HNO_3 and HCl as 16.21 and 17.18%, respectively [21]. These enhanced chemical stabilities could be attributed to the presence of rigid crystal structures, which could prevent their dissolution or leaching as heteropolyacid salts to the solution [21].

3.1.2. Thermal stability

Fig. 5 shows the effect of temperature on the skeletal structure of spinels-I ($MgAl_2O_4$) and-II ($CaAl_2O_4$). Due to prior drying, the spinels started their gradual weight loss at the same temperature at about 90–100˚C. These losses in weight are indicated by both gradual down steps and endothermic peaks described by the DTA thermograms, because of water evaporation from the surface of the powders. $MgAl_2O_4$ weight loss stopped at its offset temperature, at about 250˚C, indicating a relative stability of magnesia–alumina binary spinel than the calcium oxide–alumina system. More weight losses could be observed until 450˚C, associated with another endothermic peak, due to condensation of the crystallized water and their removal from the spinel surfaces. After 600˚C,

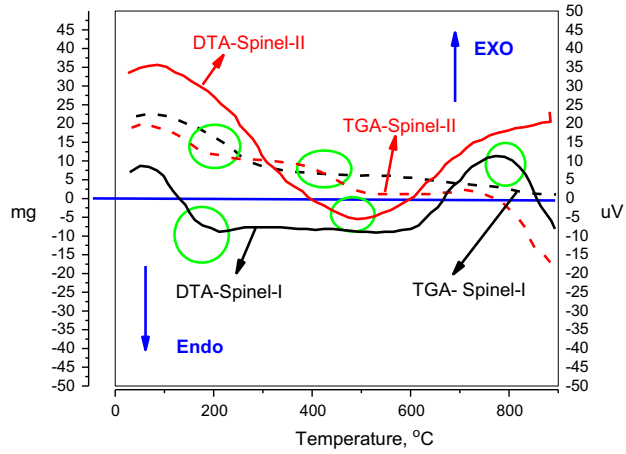

Fig. 5. DTA–TGA curves of CaO–MgO–Al_2O_3 spinels.

exothermic peaks were observed due to formation of the spinel structures, ($MgAl_2O_4$, $CaAl_2O_4$) via solid-state sintering. These data are augmented by the XRD spinels structures, as demonstrated by the joint commission of powder diffraction standards (JCPDS). Until 1,200˚C, neither further structure changes nor further weight losses (21%) were observed.

These thermogravimetric data are mostly consistent with that obtained for tin potassium vanadate (TPV) and zirconium potassium vanadate (ZPV), except for some discrepancies in their degrees and types of the weight losses. In case of TPV, the dehydration is essentially complete at 400–450˚C, and the total mass loss is 5.9%. Two stages of dehydration occur; between 20 and 90˚C due to the loss of the adsorbed water over the surface (0.4%) and between 90 and 350˚C due to the loss of water through the pores (5.5%). The result agrees well to 5.6% of water based on the structure composition. On the other hand, the weight loss in ZPV is about 4% of the sample, with delay in dehydration of water of crystallization to about 550˚C [22].

3.1.3. Functional group investigations

As shown in Fig. 5, gradual weight loss of about 3.7% observed between 351 and 550˚C as a result condensation of water molecules. These observations were augmented by the FTIR spectra indicated in Fig. 6, with some variations between the two spinels were observed. Broad band's at about 2,550–3,500 and 2,700–3,500 cm^{-1} for $MgAl_2O_4$ and $CaAl_2O_4$, respectively, with 3,200 cm^{-1} mid common centered peaks were observed, corresponding to internal water groups and some possible stretched hydroxyl moieties. The water molecules were then deformed and less broad peaks were indi-

cated at about 1,650 and 1,610 cm^{-1} for the subsequent spinels. However, the M–O bonding did not show simple spectra; doublet and multiplet spectra for $MgAl_2O_4$ and $CaAl_2O_4$ were observed below 1,000 cm^{-1}.

Similar to CaO–MgO–Al_2O_3 ternary system spinels, the FTIR spectrum of Zr(IV) tungstomolybdate indicated the presence of the extra water molecules in addition to –OH groups and metal oxides present within the material [23]. A strong and broad peak around 3,200 cm^{-1}corresponds to the presence of interstitial water and hydroxyl groups [24]. A sharp peak at 1,617 cm^{-1} corresponds to the deformation vibration of free water molecules, while the piquant peak at 1,348 cm^{-1} was due to the deformation vibration of hydroxyl groups. A broad peak in the region around 734 cm^{-1} was due to metal–oxygen bond [25].

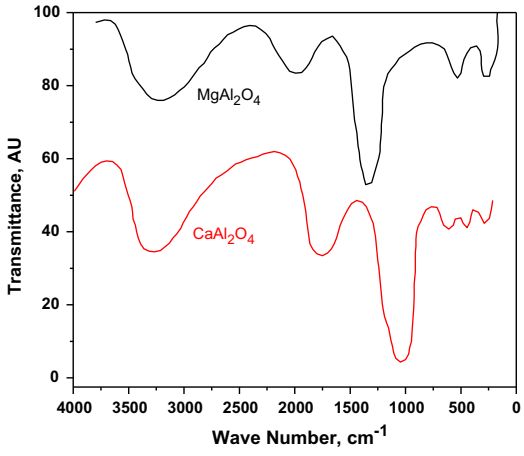

Fig. 6. FTIR spectra of CaO–MgO–Al_2O_3 ternary system at 1,900°C.

3.1.4. Crystal structural analysis

The crystal frameworks of CaO–MgO–Al_2O_3 ternary system spinels are graphically explored in Figs. 7 and 8 after identification of the XRD phases using the JCPDS of the obtained powder patterns shown in Figs. 9 and 10 and refinement of the peaks using Rietvelt methodology. The sharp peaks indicate good crystallinity of all the samples, without any impurity phase.

All the treatments present the face-centered cubic spinel. A single unit cell of normal and $CaAl_2O_4$ spinels showed a tetrahedral Mg^{2+} or Ca^{2+} coordinated by four O^{2-} ions' corner linked to a cube composed of four octahedral Al^{3+} and four O^{2-} ions. If the O^{2-} ions are considered to form a face-centred array, within the unit cell, Mg^{2+} ions occupy tetrahedral interstices between O^{2-} ions; the smaller Al^{3+} ions are cited in octahedral interstices. These cations' sublattices only partly fill the available interstices,

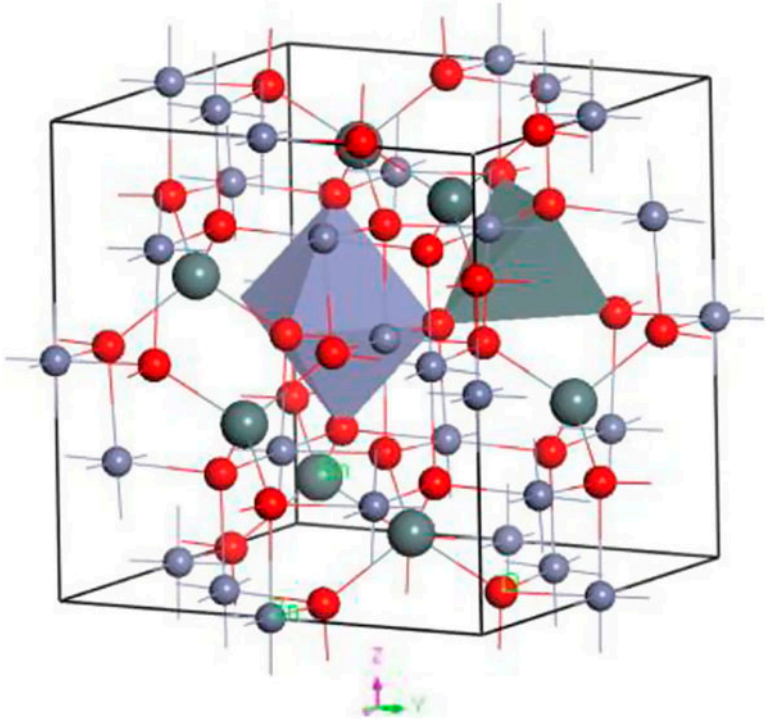

Fig. 7. Structural framework of stereoregular $CaAl_2O_4$ spinels [26].

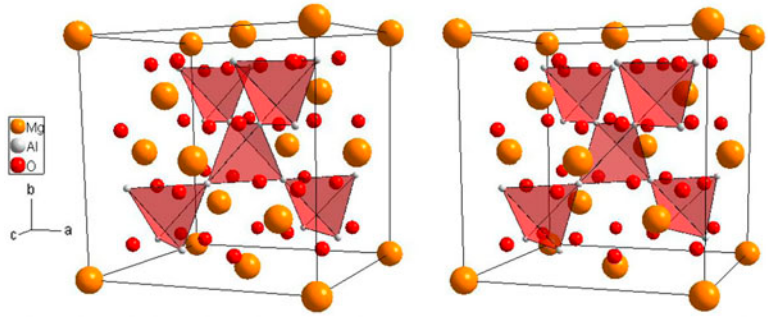

Fig. 8. Structural framework of stereoregular $MgAl_2O_4$ spinels.

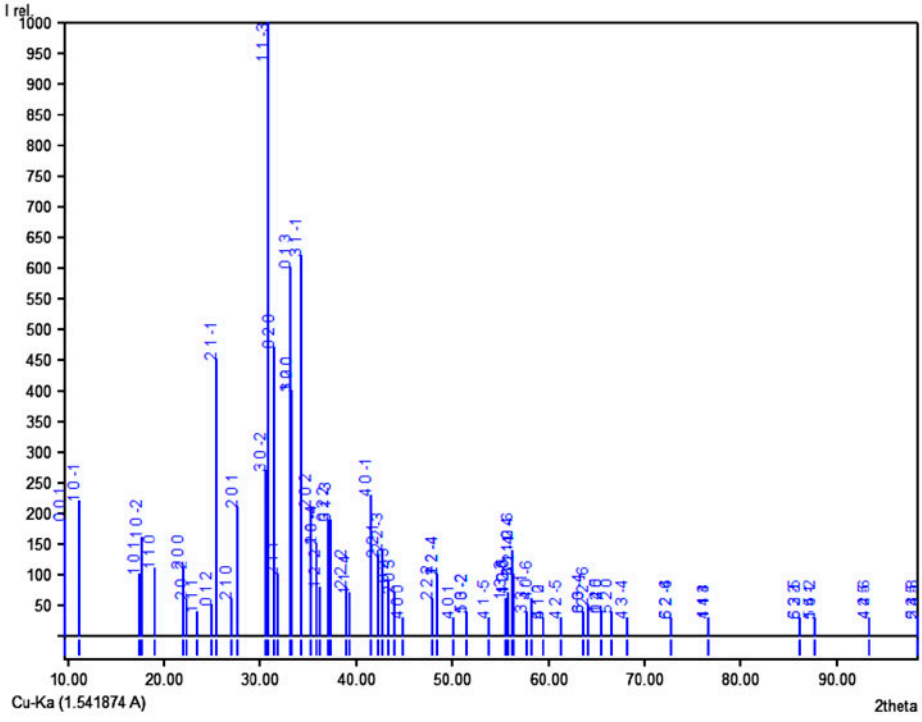

Fig. 9. XRD pattern of $CaO–Al_2O_3$ system.

and the remaining positions are generally considered to accommodate interstitial ions. Within space group, Fd 3 m Mg^{2+} or Ca^{2+} ions occupy immaculate tetrahedral 8a symmetry positions and Al^{3+} ions complete octahedral 16d, sites the O^{2-} anions occupy 48f positions, which are characterized by the oxygen positional (u) parameter, which is a measure of how far they are displaced, in ⟨1 1 1⟩ directions from ideal FCC positions. Although the observed u parameters are of how the spinel was processed, it generally corresponds to a displacement of approximately 0.1˚A. This shift is away from the divalent Mg^{2+} or Ca^{2+} ions and thus represents a volume expansion of the tetrahedral sites at the expense of octahedral site volume. These constructional data obtained in Figs. 7 and 8 are consistent with that obtained in the theoretical prediction of the configurational, electronic, and optical properties of SnB_2O_4 (B = Mg, Zn, Cd) spinels as a function of some pressure effects on their properties [26].

3.1.5. Particle size, morphology, and distribution

Figs. 11 and 12 exhibit the SEM images for $MgAl_2O_4$ and $CaAl_2O_4$ spinels with high magnification. It can be found that $CaAl_2O_4$ spinels have erratic morphology

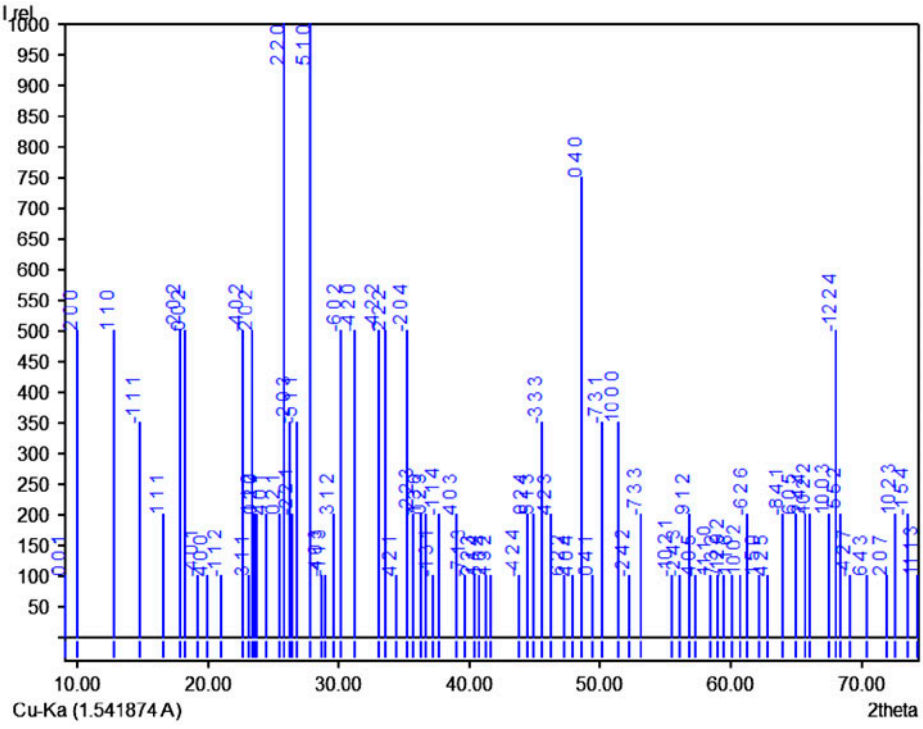

Fig. 10. XRD pattern of $MgO–Al_2O_3$ system.

and flaky-like shape. They are composed of a large number of uneven particles, and their sizes are estimated to be about 0.2 μm. Some particles happen to be reunited like one flake structure, with the average size of 0.2–0.8 μm, which is advantageous to apply in white-LED illumination. As shown in Figs. 13 and 14, the particle size, with a broad distribution from less than 60 nm to more than 250 nm, has a median value of roughly 150 nm in case of $CaAl_2O_4$, while $MgAl_2O_4$ has a spread-out distribution between about 10 and 250 nm with an average value of ca. 110 nm.

3.2. Ion exchange properties of ternary $CaO–MgO–Al_2O_3$ spinels

3.2.1. Effect of contact time

The quantity of metal ions sorbed in mg from 10^{-4} M $^{134}Cs^{+}$, $^{60}Co^{2+}$, and $^{152-154}Eu^{3+}$ onto 1 g of $MgAl_2O_4$ as a cation exchanger in aqueous solution of 0.01 M HNO_3 is shown in Fig. 15. The percent uptake was stepped up by increasing time until an individual maximum pseudo-plateau equilibrium was reached, after fitting these $^{134}Cs^{+}$, $^{60}Co^{2+}$, and

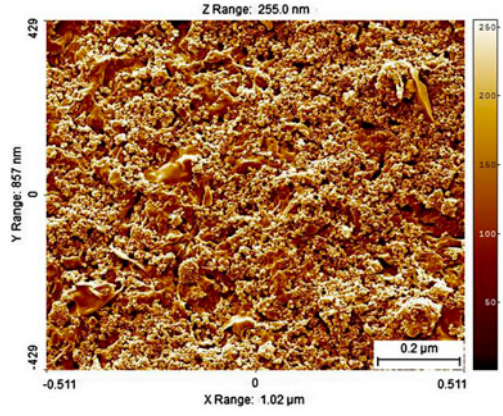

Fig. 11. 3-D SEM image of $CaAl_2O_4$ spinel.

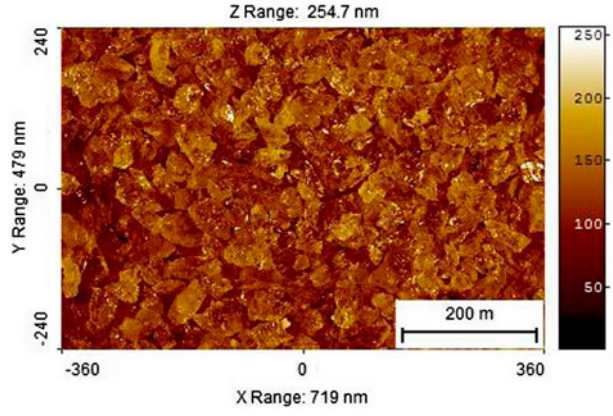

Fig. 12. 3D SEM image of $MgAl_2O_4$ spinel.

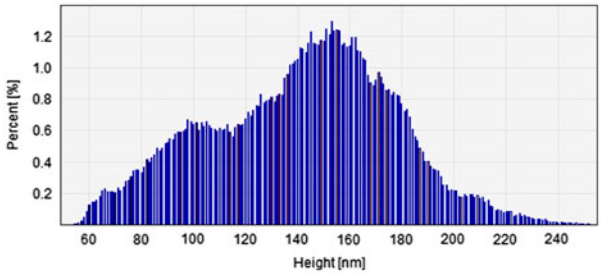

Fig. 13. Particle size distribution of $CaAl_2O_4$ spinel.

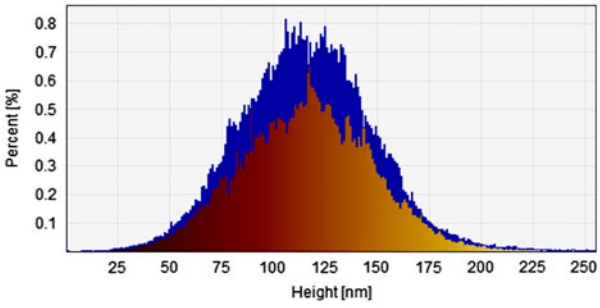

Fig. 14. Particle size distribution of $MgAl_2O_4$ spinel.

$^{152-154}Eu^{3+}$ ions curves using third-order polynomial equations. Longer reaction times have also been investigated but are not shown in Fig. 15. Consequently, 24 h was chosen, as the reaction time required reaching equilibrium in the present equilibrium sorption experiments. Under these conditions, according to Eqs. (1)–(3), the IECs for $^{134}Cs^{+}$, $^{60}Co^{2+}$, and $^{152-154}Eu^{3+}$ onto $MgAl_2O_4$ were found as 3.12, 3.35, and 3.85 meq g^{-1}, respectively.

3.2.2. Effect of pH

Fig. 16 illustrates the effect of pH in range of 1–9 on the distribution coefficient of 10^{-4} M $^{134}Cs^{+}$, $^{60}Co^{2+}$, and $^{152-154}Eu^{3+}$ onto CaO–MgO–Al_2O_3. The distribution coefficient (k_d) in mL g^{-1} is defined as the partition coefficient of the $^{134}Cs^{+}$, $^{60}Co^{2+}$, and $^{152-154}Eu^{3+}$ ions between the solid and liquid phases, respectively. The data revealed that log k_d increased by the increase of pH values, i.e. the distribution coefficient decreases with the increase of the used acid molarity.

As it could be noticed, pH can affect the surface charge of the sorbent, as well as the extent of $^{134}Cs^{+}$, $^{60}Co^{2+}$, and $^{152-154}Eu^{3+}$ solubility in the solution. Hence, the effect of solution pH on the removal efficiency of the used sorbent towards $^{134}Cs^{+}$, $^{60}Co^{2+}$, and $^{152-154}Eu^{3+}$ cations was studied by adjusting the pH of

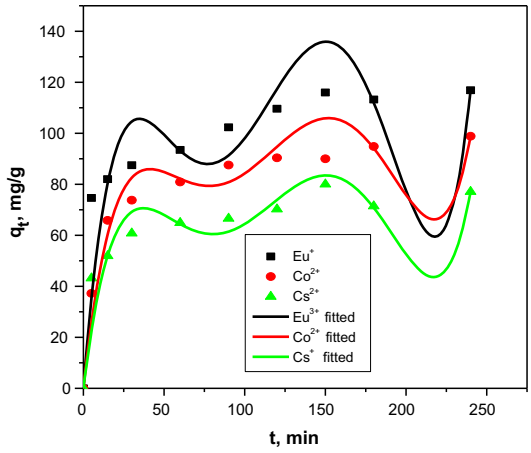

Fig. 15. Effect of contact time on the uptake of 10^{-4} M $^{134}Cs^{+}$, $^{60}Co^{2+}$, and $^{152-154}Eu^{3+}$ions by 200 mg of $MgAl_2O_4$ spinel at 298 K and about pH 3.

$^{134}Cs^{+}$, $^{60}Co^{2+}$, and $^{152-154}Eu^{3+}$ solutions before and after addition of sorbent, pH was adjusted within the diversity of 1–10 with HNO_3 and NH_3 solutions.

In strong acidic conditions, H^{+} cations compete with $^{134}Cs^{+}$, $^{60}Co^{2+}$, and $^{152-154}Eu^{3+}$ cations to occupy the ion-exchange sites of $MgAl_2O_4$ and hence, little $^{134}Cs^{+}$, $^{60}Co^{2+}$, and $^{152-154}Eu^{3+}$ cations will enter in the $MgAl_2O_4$ channels due to ion-exchange process [27]. In addition, H^{+} as a Lewis acid can occupy the free-electron pair of the negatively charged—oxygen atoms of the spinel and in short, the probability formation of $^{134}Cs^{+}$, $^{60}Co^{2+}$, and $^{152-154}Eu^{3+}$ complexes decrease. In conclusion, in piquant non-basic conditions,

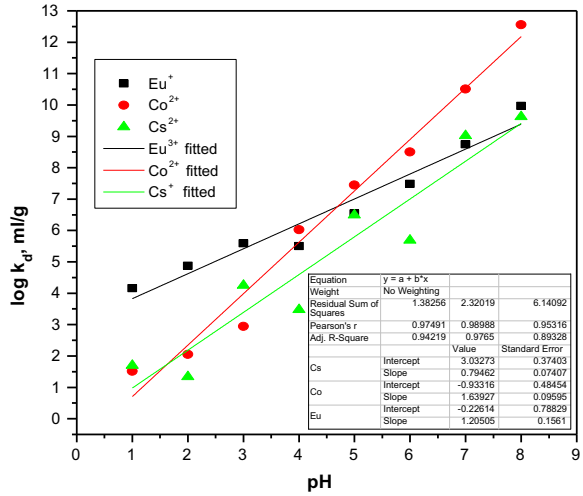

Fig. 16. Effect of pH on the distribution coefficients of 10^{-4} M $^{134}Cs^{+}$, $^{60}Co^{2+}$, and $^{152-154}Eu^{3+}$ions by 200 mg of $MgAl_2O_4$ spinel at 298 K after equilibrium for about 24 h.

due to high interference of H^+, the removal extent of $^{134}Cs^+$, $^{60}Co^{2+}$ and $^{152-154}Eu^{3+}$ cations via both ion-exchange and complexation processes decreases. Moreover, partial destruction of $MgAl_2O_4$ framework may occur at acidic pHs, which in turn decreases the removal efficiency of the sorbent towards $^{134}Cs^+$, $^{60}Co^{2+}$, and $^{152-154}Eu^{3+}$ cations [28].

Moreover, pH_{PZC} for $^{134}Cs^+$, $^{60}Co^{2+}$, and $^{152-154}Eu^{3+}$ spinel system is 6.9. At pH < pH_{PZC}, the surface of the sorbent is positively charged due to adsorption of protons, while it is negatively charged at pH > pH_{PZC}, due to adsorption of hydroxyl ions. Hence, the electrostatic repulsion between positive $^{134}Cs^+$, $^{60}Co^{2+}$, and $^{152-154}Eu^{3+}$ species and positive charges on the sorbent surface would also lead to a decrease in the removal extent of $^{134}Cs^+$, $^{60}Co^{2+}$, and $^{152-154}Eu^{3+}$ at stronger acidic conditions [29].

Hence, it is desirable with increasing pH, the interference from H^+ and also the mentioned repulsive force will decrease and removal of $^{134}Cs^+$, $^{60}Co^{2+}$, and $^{152-154}Eu^{3+}$ begin to increase. This happened by increasing pH from 1 to 4 and then the deviation is negligible to pH = 6.9. At pHs 8–9, a piquant increase in the $^{134}Cs^+$, $^{60}Co^{2+}$, and $^{152-154}Eu^{3+}$ removal was observed, which is very higher than the desirable value due to attractive electrostatic force between the positive $^{134}Cs^+$, $^{60}Co^{2+}$, and $^{152-154}Eu^{3+}$ cations and negatively surface charged at pH > pH_{PZC} [29]. On the other hand, another process is responsible for this sharp removal of $^{134}Cs^+$, $^{60}Co^{2+}$, and $^{152-154}Eu^{3+}$ cations in these pHs, which is precipitation of $^{134}Cs^+$, $^{60}Co^{2+}$, and $^{152-154}Eu^{3+}$ [30].

At more basic conditions (pH > 9), decrease in the $^{134}Cs^+$, $^{60}Co^{2+}$, and $^{152-154}Eu^{3+}$ removal can be considered as formation of bulky amine complexes $^{134}Cs^+$, $^{60}Co^{2+}$, and $^{152-154}Eu^{3+}$ due to high concentration of NH_3 in the solution [30]. As it could be seen in Fig. 16, the exact slopes for the $^{134}Cs^+$, $^{60}Co^{2+}$, and $^{152-154}Eu^{3+}/MgAl_2O_4$ were 0.79, 1.63, and 1.20, respectively. These slopes indicate mixed mechanisms rather than the pure ion-exchange route.

However, these findings are in accordance with the recorded log k_d values, 2.07, 2.04, 2.45, 2.51, 2.72, 3.21, 2.47, 2.91, 3.07, 1.92, 3.08, 3.64, 3.50, 3.13, 4.37, 3.45, 3.60, and 2.74 mL g^{-1}, respectively, obtained for Ag^+, Mg^{2+}, Ca^{2+}, Sr^{2+}, Ba^{2+}, Pb^{2+}, Cd^{2+}, Zn^{2+}, Ni^{2+}, Cu^{2+}, Co^{2+}, Cr^{3+}, Al^{3+}, Fe^{3+}, Bi^{3+}, La^{3+}, Zr^{4+}, and Th^{4+} in demineralized water as a solvent on Zr(IV) tungstomolybdate at ~pH 4 [23].

3.2.3. Sorption isotherms

Prior to studying the sorption isotherms, the effect of metal ion concentration over the range 10^{-2}–10^{-4} M on adsorption of $^{134}Cs^+$, $^{60}Co^{2+}$ and $^{152-154}Eu^{3+}/MgAl_2O_4$ in the CaO–MgO–Al_2O_3 system from 0.01 M HNO_3 medium, using equilibrium time 24 h and V/m = 200 mL g^{-1} at room temperature, was studied and graphically outlined in Fig. 17. The percent removal of $^{134}Cs^+$, $^{60}Co^{2+}$, and $^{152-154}Eu^{3+}$ decreased by expanding the metal ion concentration, while the removal efficiency stepped up isothermally by increasing the same ions concentrations. This could be explained according to Le Chatelier's principle. If a system at equilibrium is subjected to a disturbance or stress that changes any of the factors that determine the state of equilibrium, the system will reach in such a way as to eliminate the effect of this introduced disturbance [31]. Hence, with increasing $^{134}Cs^+$, $^{60}Co^{2+}$, and $^{152-154}Eu^{3+}$ content in the solution phase, equilibrium goes towards complex formation and removal of dissolved $^{134}Cs^+$, $^{60}Co^{2+}$, and $^{152-154}Eu^{3+}$ ions.

At the formative stage of the isothermal sorption process, the capacity stepped up rapidly; the $^{134}Cs^+$, $^{60}Co^{2+}$, and $^{152-154}Eu^{3+}$ adsorbed on the surface of $MgAl_2O_4$ due to surface saturation may move into porous sites. The original concentration of $^{134}Cs^+$, $^{60}Co^{2+}$, and $^{152-154}Eu^{3+}$ plays an important role to reduce the resistance to mass transfer between the solid and aqueous phases. So, the capacity is multiplied by increasing the initial $^{134}Cs^+$, $^{60}Co^{2+}$, and $^{152-154}Eu^{3+}$ concentration. In this study, Langmuir (L)—[32], Freundlich (F)—[33], Dubinin–Radushkevich (D–R)—[34], Temkin (T)—[35], Harkins–Jura (H–J)—[36], and Halsey (H)—[37] isotherm was applied to describe the equilibrium between adsorbed metal ions and metal ions in solution. The isothermal parameters of the different models were obtained by non-linear regression analysis and other parameters by linear

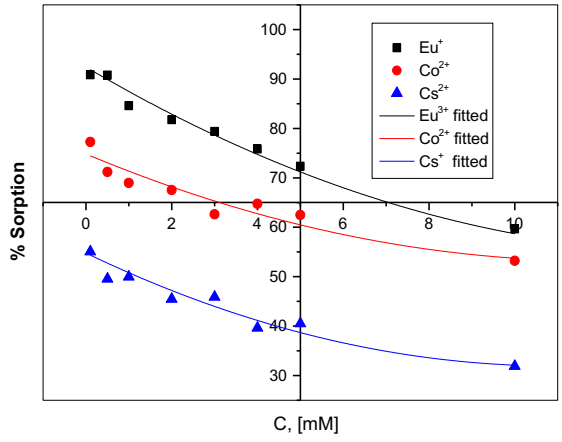

Fig. 17. Effect of ion concentration on the % sorption of $^{134}Cs^+$, $^{60}Co^{2+}$, and $^{152-154}Eu^{3+}/MgAl_2O_4$.

regression analysis using software package for statistical analysis (SPSS 14.0) and analyzed in Table 2.

The L-isotherms equation is valid for monolayer sorption on to surface [38].

$$\frac{C_e}{q_e} = \frac{1}{q_{max} k_L} + \frac{C_e}{q_{max}} \quad (4)$$

where q_e in mg g^{-1} and C_{eq} in mg L^{-1} are the amount adsorbed and the residual concentration in solution at equilibrium, correspondingly. q_{max} in mmol g^{-1} and k_L in L mg^{-1} are maximum adsorption capacity and a constant related to adsorption energy of adsorption, respectively. According to Eq. (4), the obtained maximum adsorption capacities and L-constants, calculated in Table 2, stepped up with increasing ionic charge; q_{max} for $^{134}Cs^{+}$, $^{60}Co^{2+}$, and $^{152-154}Eu^{3+}/MgAl_2O_4$ were found as 0.725, 1.110, and 1.348 mmol g^{-1}, whereas k_L values for the same elements were about 0.0625, 0.0645, and 0.0667 L mg^{-1}, respectively. On the other hand, the results of the R_L values are non-consequent; however, they indicate favorable reactions.

The F-equation is purely empirical based on sorption on a heterogeneous surface, which is commonly presented in Eq. (5) as:

$$\log q_e = \log k_F + \frac{1}{n} \log C_e \quad (5)$$

where k_F (mg g^{-1}) and n are the F-constants related to adsorption capacity and adsorption intensity, individually [33]. As it could be seen in Table 2, the sorption capacities for $^{134}Cs^{+}$, $^{60}Co^{2+}$, and $^{152-154}Eu^{3+}/MgAl_2O_4$ showed erratic trend and were about 34.67, 66.67, and 52.49 mg g^{-1}, independently. The equivalent uneven trend was found during the calculation of the intensity factors that were about 1.6748, 1.4986, and 1.6656, for the same cations, respectively.

In order to settle whether mechanism predominates, a distinction between L- and F-isothermal patterns was done. The correlation coefficients of the tested ions using L-model are about 0.9852, 0.9863, and 0.9871, while those obtained for F-model are about 0.9991, 0.9945, and 0.9998, respectively. However, these variables are not adequate to adopt F-model as the most forceful one, as the standard error estimation values slightly do not support the obtained R^2 results. Therefore, other models could be now examined to verify the most supported mechanism.

The D–R isotherm is more general than the L-isotherm, because it does not assume a homogeneous surface or constant sorption potential. The D–R equation is [34]:

Table 2
Adsorption isotherm data of various isotherm models

Parameter	Metal ions		
	$^{134}Cs^{+}$	$^{60}Co^{2+}$	$^{152-154}Eu^{3+}$
Langmuir, L constants			
q_{max} (mmol g^{-1})	0.725	1.110	1.348
k_L (L mg^{-1})	0.0625	0.0645	0.0667
R_L	0.5349	0.5788	0.4238
R^2	0.9852	0.9863	0.9871
SSE	0.0135	0.0104	0.0287
Freundlich, F constants			
K_F (mg g^{-1})	34.67	66.67	52.49
n	1.6748	1.4986	1.6656
R^2	0.9991	0.9945	0.9998
SSE	0.0036	0.0013	0.0027
Temkin, T constants			
b_T (unit-less) × 10^{-2}	4.5356	5.2756	7.1678
k_T (L $mmol^{-1}$)	0.6543	0.6250	0.5864
R^2	0.9823	0.9845	0.9758
SSE	0.5462	0.4414	0.2644
Dubinin–Redushkevich, D–R constants			
$\beta \times 10^4$	10.2113	6.1123	8.74 96
q_m (g g^{-1})	0.8603	1.3445	1.0253
E	16.4387	21.0532	18.4556
R^2	0.9886	0.9849	0.98052
SSE	0.0275	0.0035	0.0973
Harkins–Jura, H–J constants			
A	1.6358	2.5345	1.6782
B	1.0963	1.7537	1.3167
R^2	0.8735	0.8456	0.8487
SSE	0.8886	0.8855	0.7523
Halsey, H constants			
n_H	−1.6355	−1.6546	−1.8345
k_H	1.0745	1.5765	2.7435
R^2	0.8912	0.8034	0.8928
SSE	1.0886	1.1766	0.9441

$$\ln q_e = \ln q_m - \beta \varepsilon^2 \quad (6)$$

where q_e is the amount of metal adsorbed on $MgAl_2O_4$ (mmol g^{-1}), q_m is the maximum amount of metal ions that can be adsorbed under the optimized experimental conditions (mmol g^{-1}), β is a constant related to sorption energy (kJ^2 mol^{-1}), and ε is Polanyi potential, which is mathematically represented as:

$$\varepsilon = RT \ln\left(1 + \frac{1}{C_e}\right) \quad (7)$$

where R is the gas constant in kJ mol^{-1} K^{-1}, T is the absolute temperature in Kelvin, and C_e is the equilibrium concentration of metal ion in solution (mmol g^{-1}).

where ln q_e was plotted against ε^2, straight lines were observed for all the metal ions (for sleek of brevity, the figures are not shown). The values of β and q_m were computed from the slope and intercept of these straight lines. The values of β obtained were 10.2113×10^{-4}, 6.1123×10^{-4} and $8.74\ 96 \times 10^{-4}$ for $^{134}Cs^{+}$, $^{60}Co^{2+}$, and $^{152-154}Eu^{3+}$, respectively. The values of q_m for the same cations were 0.8603, 1.3445, and 1.0253 g g^{-1} individually. The value of sorption energy "E" can be correlated to β by using the following relationship.

$$E = \frac{1}{\sqrt{-2\beta}} \tag{8}$$

E is considered as the free energy of transfer of one mole of solute from infinity to the surface of $MgAl_2O_4$ spinel. This variable gives information, whether adsorption mechanism is ion exchange or physical sorption. If the magnitude of E is between 8 and 16 kJ mol^{-1}, the adsorption process follows by ion exchange, while value of $E < 8$ kJ mol^{-1}, the adsorption process is of a physical nature [39]. In the present study, the numerical values of E evaluated from Eq. (8) are 16.4387, 21.0532, and 18.4556 kJ mol^{-1} for $^{134}Cs^{+}$, $^{60}Co^{2+}$, and $^{152-154}Eu^{3+}$, respectively, which is predictable for chemisorption based on ion exchange [40].

Temkin's isotherm contains a factor that explicitly takes into account the adsorbent–adsorbate interactions. The heat of adsorption of all the molecules within the layer would decrease linearly with coverage due to adsorbent–adsorbate interactions. The adsorption is characterized by a uniform distribution of binding energies, up to some maximum binding energy [41]. The Temkin's isotherm is expressed as:

$$q_e = b_T \ln k_T + b_T \ln C_e \tag{9}$$

where b_T is Temkin's energy constant, related to the heat of adsorption by the following equation:

$$b_T = \frac{RT}{\Delta Q} \tag{10}$$

where R is the ideal gas constant (8.314×10^{-3} kJ K^{-1} mol^{-1}), T is the absolute temperature (K), and ΔQ is related to the heat of adsorption (equivalent to $-\Delta H_{ads}$). k_T is Temkin equilibrium binding constant (L $mmol^{-1}$) expressed as

$$k_T = k_0 \exp(\Delta Q_0 / RT) \tag{11}$$

where Q_0 is the lowest characteristic heat of adsorption and k_0 is a constant; low k_T values indicate low adsorbate–adsorbate interactions.

This isotherm cannot be used for very small quantities of sorbed gas or ions because the limit of the $q(P$ or $C_e)$ function when P or C_e tends to zero is:

$$\lim_{C \to 0} q = \lim_{C \to 0} q_m \frac{RT}{\Delta Q} \ln kTC_e = -\infty \tag{12}$$

This equation (cf. Eq. 12) shows that the isotherm has no physical sense for very low pressure or concentration. Furthermore, when the heterogeneity of the surface lowers and when $\Delta Q/RT$ reaches zero, the equation of Temkin also loses any physical meaning inasmuch as q approaches infinity at any pressure or concentration [42]. According to Table 2, the heat of adsorption could be obtained after estimation of the b_T constant of $^{134}Cs^{+}$, $^{60}Co^{2+}$, and $^{152-154}Eu^{3+}/MgAl_2O_4$, as 4.5356×10^2, 5.2756×10^2, and 7.1678×10^2, respectively. According to Eq. (10), the heats of adsorptions are inversely proportional to b_T; ΔQ values increase in the following order $^{134}Cs^{+} > {}^{60}Co^{2+} > {}^{152-154}Eu^{3+}$, which indicates the hydration of the mentioned ions. On the other hand, the equilibrium binding constants are non-consequent and have the values of 0.6543, 0.6250, and 0.5864 L $mmol^{-1}$, respectively. The correlation coefficients of Temkin's equation could be approved. The low values of ΔQ (0–10 J mol^{-1}) could be explained by adsorbate–adsorbate interactions rather than adsorbate–adsorbent interactions, regardless the type of adsorption, physical or chemical.

H–J proposed a unique expression between the amount sorbed in mg g^{-1} and the equilibrium concentration in mmol L^{-1} as [36]:

$$\frac{1}{q_e^2} = \left[\frac{B}{A}\right] - \left[\frac{1}{A}\right] \log C_e \tag{13}$$

where A and B are the constants calculated from the slope and intercept of the linear plot between $1/{q_e}^2$ and log C_e. The isotherm equation also accounts for multilayer adsorption and explains the existence of a heterogeneous pore distribution. The obtained A values for $^{134}Cs^{+}$, $^{60}Co^{2+}$, and $^{152-154}Eu^{3+}/MgAl_2O_4$ were about 1.6358, 2.5345, and 1.6782, while the B values for the same cations were about 1.0963, 1.7537, and 1.3167, respectively. The corresponding correlation coefficients as well as the standard deviations were recorded as R^2 (0.8735, 0.8456, and 0.8487) and SSE (0.8886, 0.8855, and 0.7523), individually.

Halsey proposed an expression for condensation of a multilayer process at a relatively large distance from the surface [37]:

$$\ln q_e = \left[\frac{1}{n_H}\ln k_H\right] - \left[\frac{1}{n_H}\ln C_e\right] \quad (14)$$

In that model, the analysis of adsorption on a uniform surface using the quasi-chemical theory of interaction showed that the conjectures of the BET theory led substantially to no adsorption beyond the first layer if $E_2 = E_L$, and stepwise isotherms if $E_1 > E_2 > E_3 >> E_L$. Harmonizing to Halsey, the monolayer adsorption of some gases on silver, platinum, and steel, the heterogeneous nature of the adsorbing surface could be interpreted. Adsorption on the non-uniform surface was treated, and the collaborative of the F-equation was derived. Illustrative multi-layer isotherm could be considered that composed of three regions: non-cooperative adsorption on a strongly heterogeneous surface; cooperative adsorption on a still heterogeneous surface; illustrative multilayer adsorption induced by small van der Waals perturbations on some distance from the surface. The isotherm $p/\mathring{p} = \exp\{-a/\theta r\}$ is derived and shown to be a good representation of adsorption data that conform to the BET Type I, II, or III shapes. A linear plot between log q_e vs log C_e gives the values of Halsey's constants n_H and k_H from the slopes and intercepts, respectively. As could be seen in Table 2, the adsorption constants for $^{134}Cs^+$, $^{60}Co^{2+}$, and $^{152-154}Eu^{3+}/MgAl_2O_4$ were recorded as n_H (−1.6355, −1.6546, and −1.8345) and k_H (1.0745, 1.5765, and 2.7435), respectively, indicating low tendency of the mentioned ions to be multilayer arranged over the spinel surface. Similar to H–J, Halsey's model explained multilayer adsorption. H–J and Halsey's models exhibit highly low R^2 values and deeply high SSE value indicating that the adsorption process follows fairly these models.

3.2.4. Thermodynamics of adsorption

The influence of temperature on the adsorption of various metal ions on $MgAl_2O_4$ spinel was also studied in optimized conditions. The temperature varied from 20 to 50°C. The adsorption of $^{134}Cs^+$, $^{60}Co^{2+}$, and $^{152-154}Eu^{3+}/MgAl_2O_4$ stepped up with decreasing the reaction temperature. This is due to the exothermic nature of different valence cations [43]. As a regular ion-exchange dependence, the surface energy of the Al_2O_4 spinel should increase with temperature; however, the reaction mechanism as ion exchange is now excluded due to this behavior [43,44].

The values of ΔH^{ads}, ΔS^{ads}, and ΔG^{ads} were also calculated from the slope and intercept of the Van't Hoff plot of the adsorption of $^{134}Cs^+$, $^{60}Co^{2+}$, and $^{152-154}Eu^{3+}/MgAl_2O_4$, i.e. the linear variation of ln K with reciprocal temperature $1/T$ (Fig. 18) using the following relation (Eq. (15)):

$$\ln K = \frac{\Delta S^{ads}}{R} - \frac{\Delta H^{ads}}{RT} \quad (15)$$

where K is the equilibrium reaction constant, ΔS^{ads} is the entropy change for the process, and ΔH^{ads} is the enthalpy change for the process. The free energy of the adsorption and ΔG^{ads} was calculated using the following Van't Hoff equation:

$$\Delta G^{ads} = -RT\ln K \quad (16)$$

The determination of the thermodynamic parameters for the adsorption of various $^{134}Cs^+$, $^{60}Co^{2+}$, and $^{152-154}Eu^{3+}/MgAl_2O_4$ spinel is given in Table 3. The value of ΔH^{ads} is negative, which indicates an exothermic adsorption process, and it indicates that the chelation mechanism dominates [45]. The entropy (ΔS^{ads}) is positive corresponding with an increase in degree of freedom of the system due to release of hydrogen ions for the different valence metal ions under study [46]. The negative values of ΔG^{ads} indicate the feasibility of the process and the spontaneity of the adsorption process. The amount of metal ions adsorbed at equilibrium must decrease with increasing

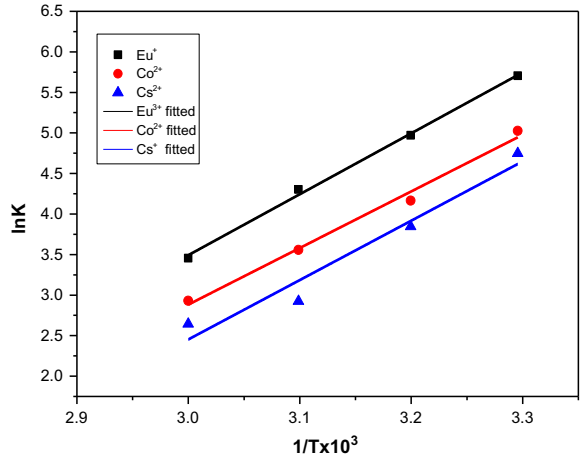

Fig. 18. Effect of reaction temperature on the equilibrium constant of $^{134}Cs^+$, $^{60}Co^{2+}$, and $^{152-154}Eu^{3+}/MgAl_2O_4$ spinel.

Table 3
Thermodynamic parameters for $^{134}Cs^{+}$, $^{60}Co^{2+}$, and $^{152-154}Eu^{3+}$/$MgAl_2O_4$ spinel

Metal ions	T (K)	1/T (K^{-1})	K	ln K	ΔG^{ads} (kJ $mol^{-1)}$	ΔH^{ads} (kJ mol^{-1})	ΔS^{ads} (J K^{-1} mol^{-1})
$^{134}Cs^{+}$	293	3.30×10^{-3}	1,305,661	14.08222	−33.7514	−26.1344	112.9575
	303	3.19×10^{-3}	993490.7	13.80898	−34.2261		
	313	3.09×10^{-3}	331008.7	12.7099	−32.5417		
	323	3.00×10^{-3}	73580.84	11.20614	−29.6082		
$^{60}Co^{2+}$	293	3.30×10^{-3}	11,385,259	16.24783	−38.9418	−27.2677	119.0434
	303	3.19×10^{-3}	2,090,638	14.55298	−36.0701		
	313	3.09×10^{-3}	216,776	12.28662	−31.4579		
	323	3.00×10^{-3}	93621.94	11.44702	−30.2446		
$^{152-154}Eu^{3+}$	293	3.30×10^{-3}	91,600,748	18.33295	−43.9393	−27.4562	138.2785
	303	3.19×10^{-3}	21,954,002	16.90446	−41.8984		
	313	3.09×10^{-3}	7,608,830	15.84482	−40.5681		
	323	3.00×10^{-3}	1,463,425	14.19629	−37.5086		

temperatures, because ΔG^{ads} increases with the rise in temperature of the solution [47].

4. Conclusion

$CaO–MgO–Al_2O_3$ ternary system was utilized as a key system for preparation of some chemical formulations as $Ca_3MgAl_4O_{10}$, $Ca_3Al_2O_6$, $CaMg_2Al_{16}O_{27}$, $Ca_2Mg_2Al_{26}O_{45}$, corundum, periclase and monoxide lime at room temperature, $MgAl_2O_4$ spinel at 1,200–1,400˚C and $MgAl_2O_4$ spinel at 1,725–1,900˚C. $CaAl_2O_4$ and $MgAl_2O_4$ are chemically and thermally stable in their spinel configurations. They have different surface, morphological, and topographical structures. Due to its appropriate characteristics, $MgAl_2O_4$ was anticipated for removal of $^{134}Cs^{+}$, $^{60}Co^{2+}$, and $^{152-154}Eu^{3+}$ from waste solutions. $MgAl_2O_4$ possessed higher roughness, higher surface area, and more homogeneous particle size distributions than those of $CaAl_2O_4$. The time dependency investigations suggested 24 h as an equilibrium time. L, F, D–R, T, H–J, and H- isotherms were put together to describe the equilibrium between adsorbed metal ions and metal ions in solution at different concentrations. The values of E were about 16.4387, 21.0532, and 18.4556 kJ mol^{-1} for $^{134}Cs^{+}$, $^{60}Co^{2+}$, and $^{152-154}Eu^{3+}$, respectively, which is predictable for chemisorption based on ion exchange. The consequent isothermal models augmented these predictions; some adsorbate–adsorbate interactions were also detected. The sorption of $^{134}Cs^{+}$, $^{60}Co^{2+}$, and $^{152-154}Eu^{3+}$ was critically affected by temperature; spontaneous and exothermic nature and positive entropy of sorption was found at specific pH values. Based on isothermal and thermodynamic data, chemical reaction based on ion exchange rather than pure ion exchange mechanism predominates.

References

[1] P.K. Mohapatra, A. Bhattacharyya, V.K. Manchanda, Selective separation of radio-cesium from acidic solutions using supported liquid membrane containing chlorinated cobalt dicarbollide (CCD) in phenyltrifluoromethyl sulphone (PTMS), J. Hazard. Mater. 18 (2010) 679–685.
[2] R.S. Herbst, J.D. Law, T.A. Todd, V.N. Romanovskiy, I.V. Smirnov, V.A. Babain, V.N. Esimantovskiy, B.N. Zaitsev, Development of the universal extraction (UNEX) process for the simultaneous recovery of Cs, Sr and actinides from acidic radioactive wastes, Sep. Sci. Technol. 38 (2003) 2685–2708.
[3] E.H. Borai, R. Harjula, L. Malinen, A. Paajanen, Efficient removal of cesium from low-level radioactive liquid waste using natural and impregnated zeolites minerals, J. Hazard. Mater. 172 (2009) 416–422.
[4] T. Möller, R. Harjula, P. Kelokaski, K. Vaaramaa, P. Karhu, J. Lehto, Titanium antimonates in various Ti:Sb ratios: Ion exchange properties for radionuclide ions, J. Mater. Chem. 13 (2003) 535–541.
[5] L. Al-Attar, A. Dyer, A. Paajanen, R. Harjula, Purification of nuclear wastes by novel inorganic ion exchangers, J. Mater. Chem. 13 (2003) 2969–2974.
[6] A. Dyer, J. Newton, L. O'Brien, S. Owens, Studies on a synthetic sitinakite-type silicotitanate cation exchanger. Part 2. Effect of alkaline earth and alkali metals on the uptake of Cs and Sr radioisotopes, Microporous Mesoporous Mater. 120 (2009) 272–277.
[7] K. Popa, C.C. Pavel, Radioactive wastewaters purification using titanosilicates materials: State of the art and perspectives, Desalination 293 (2012) 78–86.
[8] T. Möller, A. Clearfield, R. Harjula, Preparation of hydrous mixed oxides of Sb, Nb, Si, Ti and W with a pyrochlore structure and exchange of radioactive cesium and strontium ions into the materials, Microporous Mesoporous Mater. 54 (2002) 187–199.
[9] C.S. Griffith, V. Luca, Ion-exchange properties of microporous tungstates, Chem. Mater. 16 (2004) 4992–4999.
[10] Y. Park, Y.C. Lee, W.S. Shin, S.J. Choi, Removal of cobalt, strontium and cesium from radioactive laundry wastewater by ammonium molybdophosphate–poly-

acrylonitrile (AMP–PAN), Chem. Eng. J. 162 (2010) 685–695.
[11] C. Delchet, A. Tokarev, X. Dumail, G. Toquer, Y. Barre, Y. Guari, C. Guerin, J. Larionova, A. Grandjean, Extraction of radioactive cesium using innovative functionalized porous materials, RSC Adv. 2 (2012) 5707–5716.
[12] T. Sangvanich, V. Sukwarotwat, R.J. Wiacek, R.M. Grudzien, G.E. Fryxell, R.S. Addleman, C. Timchalk, W. Yantasee, Selective capture of cesium and thallium from natural waters and simulated waste with copper ferrocyanide functionalized mesoporous silica, J. Hazard. Mater. 182 (2010) 225–231.
[13] C. Dwivedi, A. Kumar, J.K. Ajish, K.K. Singh, M. Kumar, P.K. Wattal, P.N. Bajaj, Resorcinol-formaldehyde coated XAD resin beads for removal of cesium ions from radioactive waste: Synthesis, sorption and kinetic studies, RSC Adv. 2 (2012) 5557–5564.
[14] C.Y. Chang, L.K. Chau, W.P. Hu, C.Y. Wang, J.H. Liao, Nickel hexacyanoferrate multilayers on functionalized mesoporous silica supports for selective sorption and sensing of cesium, Microporous Mesoporous Mater. 109 (2008) 501–512.
[15] V. Avramenko, S. Bratskaya, V. Zheleznov, I. Sheveleva, O. Voitenko, V. Sergienko, Colloid stable sorbents for cesium removal: Preparation and application of latex particles functionalized with transitional metals ferrocyanides, J. Hazard. Mater. 186 (2011) 1343–1350.
[16] R. Yavari, S.J. Ahmadi, Y.D. Huang, A.R. Khanchi, G. Bagheri, J.M. He, Synthesis, characterization and analytical application of a new inorganic cation exchanger-titanium (IV) molybdophophate, Talanta 77 (2009) 1179–1184.
[17] S.A. Nabi, M. Naushad, A new electron exchange material Ti (IV) iodovanadate: Synthesis, characterization and analytical applications, Chem. Eng. J. 158 (2010) 100–107.
[18] Z.M. Siddiqi, D. Pathania, Titanium (IV) tungstosilicate and titanium (IV) tungstophophate: Two new inorganic ion exchangers, J. Chromatogr. A 987 (2003) 147–158.
[19] L. Wang, W. Ma, R. Liu, H.Y. Li, C.G. Meng, Correlation between Li^+ adsorption, capacity and the preparation conditions of spinel lithium manganese precursor, Solid State Sci. 177 (2006) 1421–1428.
[20] K. Lv, L.P. Xiong, Y.M. Luo, Ion exchange properties of cesium ion sieve based on zirconium molybdopyrophosphate, Colloids Surf. A 433 (20) (2013) 37–46.
[21] I.M. El-Naggar, G.M. Ibrahim, B. El-Gammal, E.A. El-Kady, Integrated synthesis and characterization of some porous polyacrylamide-based composites for cationic sorption from aqueous liquid wastes, Desal. Water Treat. (2013).
[22] G.M. Ibrahim, B. El-Gammal, I. M. El-Naggar, Synthesis and characterization of novel materials tin potassium vanadate and zirconium potassium vanadate inorganic multi-component ion exchangers, Sep. Sci. Technol. 46 (2011) 664–678.
[23] S.A. Nabi, M. Naushad, Inamuddin, Synthesis and characterization of a new inorganic cation-exchanger —Zr(IV) tungstomolybdate: Analytical applications for metal content determination in real sample and synthetic mixture, J. Hazard. Mater. 142 (1–2) (2007) 404–411.
[24] G. Socrates, Infrared Characteristic Group Frequencies, John Wiley, New York, NY, 1980, pp. 145–150.
[25] G. Alberti, E. Toracca, E. Conte, Influence of thermal treatment on the rate of ion-exchange of zirconium phosphate, J. Inorg. Nucl. Chem. 28 (1966) 607–613.
[26] D. Allali, A. Bouhemadou, S. Bin-Omran, Theoretical prediction of the structural, electronic and optical properties of SnB_2O_4 (B=Mg, Zn, Cd), Comput. Mater. Sci. 51 (1) (2012) 194–205.
[27] W. Chunfeng, L. Jiansheng, S. Xia, W. Lianjun, S. Xiuyun, Evaluation of zeolites synthesized from fly ash as potential adsorbents for wastewater containing heavy metals, J. Environ. Sci. 21 (2009) 127–136.
[28] V.J. Inglezakis, M. Stylianou, M. Loizidou, Ion exchange and adsorption equilibrium studies on clinoptilolite, bentonite and vermiculite, J. Phys. Chem. Solids 71 (2010) 279–284.
[29] H. Zhang, X. Yu, L. Chen, Y. Jing, Z. Ge, Study of ^{63}Ni adsorption on NKF-6 zeolite, J. Environ. Radioact. 101 (2010) 1061–1069.
[30] H.S. Ibrahim, T.S. Jamil, E.Z. Hegazy, Application of zeolite prepared from *Egyptian kaolin* for the removal of heavy metals: II. Isotherm models, J. Hazard. Mater. 182 (2010) 842–847.
[31] K.L. Lin, B.Y. Chen, Understanding biotoxicity for reusability of municipal solid waste incinerator (MSWI) ash, J. Hazard. Mater. 138 (2006) 9–15.
[32] I. Langmuir, The constitution and fundamental properties of solids and liquids. Part I. Solids, J. Am. Chem. Soc. 38 (1916) 2221–2295.
[33] H.M.F. Freundlich, Ober die adsorption in Lösungen, Z. Phys. Chem. (Leipzig) 57 (1906) 385–470.
[34] M.M. Dubinin, B. Radushkevich, Equation of the characteristic curve of activated charcoal, Chem. Zentralbl. 1 (1947) 875–881.
[35] M.I. Temkin, V. Pyzhev, Kinetics of ammonia synthesis on promoted iron catalysts, Acta Physiochim URSS 12 (1940) 327–356.
[36] W.D. Harkins, G. Jura, An adsorption method for the determination of the area of a solid without the assumption of a molecular area, and the area occupied by nitrogen molecules on the surfaces of solids [3], J. Chem. Phys. 11 (1943) 431–432.
[37] G. Halsey, Physical adsorption on non-uniform surfaces, J. Chem. Phys. 16 (1948) 931–937.
[38] J.M. Smith, Chemical Engineering Kinetics, 3rd ed. McGraw-Hill, Singapore, 1981.
[39] A.S. Özcan, B. Erdem, A. Özcan, Adsorption of acid blue 193 from aqueous solutions onto BTMA-bentonite, Colloids Surf. A 266 (1–3) (2005) 73–81.
[40] N. Khalid, S. Ali, S. Pervez, Sorption potential of styrene-divinylbenzene copolymer beads for the decontamination of lead from aqueous media, Sep. Sci. Technol. 42 (2007) 203–222.
[41] C. Garnier, G. Finqueneisel, T. Zimny, Z. Pokryszka, S. Lafortune, P.D.C. Défossez, E.C. Gaucher, Selection of coals of different maturities for CO_2 Storage by modelling of CH4 and CO_2 adsorption isotherms, Int. J. Coal Geol. 87 (1, 2) (2011) 80–86.
[42] L.D. Asnin, A.A. Fedorov, Y.S. Chekryshkin, Thermodynamic parameters of adsorption described by the logarithmic Temkin isotherm, Russ. Chem. Bull. 50 (2001) 217–219.

[43] E. Pehlivan, T. Altun, The study of various parameters affecting the ion exchange of Cu2+, Zn2+, Ni2+, Cd2+, and Pb2+ from aqueous solution on Dowex 50 W synthetic resin, J. Hazard. Mater. 134 (1–3) (2006) 149–156.
[44] A. Demirbas, E. Pehlivan, F. Gode, T. Altun, G. Arslan, Adsorption of Cu(II), Zn(II), Ni(II), Pb(II), and Cd(II) from aqueous solution on Amberlite IR-120 synthetic resin, J. Colloid Interface Sci. 282 (1) (2005) 20–25.
[45] I.S. Lima, C. Airoldi, A thermodynamic investigation on chitosan-divalent cation interactions, Thermochim. Acta 421 (1–2) (2004) 133–139.
[46] A. Baraka, P.J. Hall, M.J. Heslop, Melamine–formaldehyde–NTA chelating gel resin: Synthesis, characterization and application for copper (II) ion removal from synthetic wastewater, J. Hazard. Mater. 140 (1–2) (2007) 86–94.
[47] G. Karthikeyan, K. Anbalagan, N.M. Andal, Adsorption dynamics and equilibrium studies of Zn(II) onto chitosan, J. Chem. Sci. 116 (2004) 119–127.